Investigative power of Genomic Informational Field Theory (GIFT) relative to GWAS for genotype-phenotype mapping

Citation for published version:
Kyratzi, P, Matika, O, Brassington, AH, Connie, CE, Xu, J, Barrett, DA, Emes, RD, Archibald, AL, Paldi, A, Sinclair, KD, Wattis, J & Rauch, C 2024 'Investigative power of Genomic Informational Field Theory (GIFT) relative to GWAS for genotype-phenotype mapping' bioRxiv, bioRxiv, pp. 1-27.
https://doi.org/10.1101/2024.04.16.589524

Digital Object Identifier (DOI):
10.1101/2024.04.16.589524

Link:
Link to publication record in Edinburgh Research Explorer

Document Version:
Publisher's PDF, also known as Version of record

Investigative power of Genomic Informational Field Theory (GIFT) relative to GWAS for genotype-phenotype mapping

Panagiota Kyratzi[1,2], Oswald Matika[3], Amey H Brassington[4], Clare E Connie[5], Juan Xu[6], David A Barrett[7], Richard D Emes[8], Alan L Archibald[3], Andras Paldi[2], Kevin D Sinclair[4], Jonathan Wattis[9] and, Cyril Rauch[1]

[1] School of Veterinary Medicine and Science, University of Nottingham, College Road, Sutton Bonington, LE12 5RD, UK.

[2] École Pratique des Hautes Études, PSL Research University, St-Antoine Research Center, Inserm U938, 34 rue Crozatier, 75012 Paris, France.

[3] Div. Genetics and Genomics, The Roslin Institute and Royal (Dick) School of Veterinary Studies, University of Edinburgh, Easter Bush, Midlothian EH25 9RG, Scotland, UK

[4]Agriculture and Horticulture Development Board, Middlemarch Business Park Siskin Parkway, East Coventry CV3 4PE, UK.

[5] School of Biosciences, University of Nottingham, College Road, Sutton Bonington, LE12 5RD, UK.

[6] Shanghai Leadingtac Pharmaceutical Co., Ltd, 781 Cailun Road, China (Shanghai) Pilot Free Trade Zone, Pudong, Shanghai 201203, China

[7] Centre for Analytical Bioscience, School of Pharmacy, University of Nottingham, Nottingham NG7 2RD, UK.

[8] Nottingham Trent University, 50 Shakespeare Street, Nottingham NG1 4FQ, UK.

[9] Centre for Mathematical Medicine and Biology, School of Mathematical Sciences, University of Nottingham, University Park, Nottingham NG7 2RD, UK.

Corresponding author: cyril.rauch@nottingham.ac.uk

Keywords: GIFT, genotype-phenotype mapping, GWAS

Abstract

Identifying associations between phenotype and genotype is the fundamental basis of genetic analyses. Inspired by frequentist probability and the work of R.A. Fisher, genome-wide association studies (GWAS) extract information using averages and variances from genotype-phenotype datasets. Averages and variances are legitimated upon creating distribution density functions obtained through the grouping of data into categories. However, as data from within a given category cannot be differentiated, the investigative power of such methodologies is limited. Genomic Informational Field Theory (GIFT) is a method specifically designed to circumvent this issue. The way GIFT proceeds is opposite to that of GWAS. Whilst GWAS determines the extent to which genes are involved in phenotype formation (bottom-up approach), GIFT determines the degree to which the phenotype can select microstates (genes) for its subsistence (top-down approach). Doing so requires dealing with new genetic concepts, a.k.a. genetic paths, upon which significance levels for genotype-phenotype associations can be determined. By using different datasets obtained in *ovis aries* related to bone growth (Dataset-1) and to a series of linked metabolic and epigenetic pathways (Dataset-2), we demonstrate that removing the informational barrier linked to categories enhances the investigative and discriminative powers of GIFT, namely that GIFT extracts more information than GWAS. We conclude by suggesting that GIFT is an adequate tool to study how phenotypic plasticity and genetic assimilation are linked.

Introduction

Identifying associations between phenotype and genotype is the fundamental basis of genetic analysis. The development of high-density genotyping and whole genome sequencing has enabled DNA variants to be directly identified and Genome-Wide Association Studies (GWASs) have become the method of choice for mapping genotype to phenotype in large populations of unrelated individuals. GWAS have been employed in many species, and especially in the study of human disease (1). By 2021 the NHGRI-EBI GWAS Catalog listed 316,782 associations identified in 5149 publications describing GWAS results (2). Additionally, extensive collection of data has been initiated through efforts such as the UK Biobank (3), Generation Scotland (4) and NIH *All of Us* research program (https://allofus.nih.gov/) in the expectation that large-scale GWAS will elucidate the basis of human health and disease and facilitate precision medicine.

While genomic technologies have advanced rapidly, statistical models used to analyse genetic data are still based on the models developed by Fisher more than 100 years ago (5,6). GWASs essentially make use of the Fisher method of partitioning genotypic values by performing a linear regression of phenotype on marker allelic dosage (7). Regression coefficients estimate the average allele effect size, and the regression variance is the additive genetic variance due to the locus (8). However, an ongoing debate exists over whether the present analysis paradigm in quantitative genetics is at its limits for truly understanding complex traits, namely traits resulting from many genes each with very small effect size (9). As a result, one may wonder whether alternative statistical model(s) could be invented and used to determine genotype-phenotype mappings.

GWASs are fundamentally linked to frequentist probabilities that, defined through relative frequencies, determines the validity of statistical inferences. In practice, frequentist probabilities are generated through the grouping of data into bins or categories to generate a bar chart, that is then interpolated to create a distribution density function (DDF) in the continuum limit. The DDF is, in turn, used to determine statistical inferences including average, variance, p-value and so on. However, since the DDF approximates the bar chart (and not the converse), and that it is not possible to differentiate data from within any given group/category, the DDF is constructed mathematically on the implicit assumption that information is missing to differentiate data from within any given group/category.

The notion of 'missing information' can be legitimate and defined experimentally. For example, measuring the phenotype, human height with a ruler with centimetre graduations implies that any height can be measured to the nearest centimetre. Consequently, one centimetre-width bins/categories need to be used to generate a frequency table of range of phenotype values upon which the phenotype and genotype DDFs are defined. In this case, all the resulting statistical inferences are defined with a precision corresponding to the nearest centimetre. The 'missing information' (i.e., that what cannot be measured by the ruler) corresponds then to sub-centimetric scales (i.e., distances to the nearest millimetre for this example). In practice the 'missing information' is therefore linked to the one of 'imprecision' and deciding to provide more precise statistical inferences implies that the width of categories be reduced, which can only be achieved by increasing the sample size. It is not by chance that the 'normal distribution' created by mathematicians and physicists was initially called the 'law of errors', where the notion of error (misinformation) results from imprecisions in experimental measurements. As a result, GWAS is faced with a fundamental issue involving the extraction of precise information using a method that, conceptually, assumes that information is missing or that data is mis-(in)formed.

In general, the problem concerning the 'missing information' is never mentioned since the DDF in the continuum limit is never considered as an approximation but as something that has its own reality. Namely a DDF must exist independently of data measured (i.e., data must fit the DDF and not the converse). The latter remark leads to an interesting conceptual territory where the notions of average and variance, and their usage, may be questioned. If one considers the normal distribution (or any other DDFs) is inherent to life and that data must fit it (them), then the moments of the distribution (e.g., average and variance) are also essential parameters to describe life, and the variance often interpreted as noise in the data is then a nuisance. If, on the contrary, data is the important thing, and that the DDF is considered solely as a tool to interpolate data based on missing information, then average and variance are parameters derived from a lack of information and are, as a result, poorly informative. The latter point should not come as a surprise as reducing the huge diversity of populations to a handful of parameters (i.e., average and variance) is highly reductionist and likely to be poorly descriptive. Thus, while the notions of average and variance may help representing datasets, they are inventions nonetheless (i.e., thought constructions akin to the field of frequentist probability. Thus, using average and variance as a starting point to map genotype-phenotype (GWAS) is a matter of choice. Accordingly, different statistical methods can be suggested.

To avoid those conceptual and practical issues a new method called GIFT (Genomic Informational Field Theory) has been designed (10,11), reviewed in (12). In short, to associate genotype to phenotype GIFT does not presume that the only important information concerning the gene effect is found in averages or variances, nor does it presume that DDFs are central. On the contrary, GIFT starts with the pre-requisite that phenotypic values, or phenotypic residuals after considering the environment/fixed effects, may be measured with sufficient precision to be unique in a population. Then, by avoiding grouping data into bins/categories, which would otherwise create an artificial imprecision, GIFT considers the entire information contained in the data, (i.e., variance is not a nuisance anymore) making use of the cumulative sum of microstates. Figure 1 provides the intuition underscoring GIFT as a method.

In the current article we demonstrate the informational/investigative power of GIFT relative to GWAS using two different datasets:

i. Dataset-1 is derived from a study concerned with the genetic background of carcass composition in sheep (*ovis aries*) (13). Using GWAS this study demonstrated a strong association between chromosome 6 and the carcass composition trait 'bone area at the ischium'. We now apply GIFT to this dataset such as to benchmark it against GWAS. Since GWAS has already informed the genetic background of the trait, we expect GIFT to at least replicate GWAS results.
ii. Dataset-2 concerns biochemical data arising from an ongoing study in sheep which seeks to identify risk allele variants in genes whose products direct a series of metabolic pathways, collectively referred to as one carbon (1C) metabolism, and associated epigenetic regulators. The gene array was designed in such a way to include all the single nucleotide polymorphisms (SNPs) linked to known biochemical enzymes involved in these pathways. Given that Dataset-2 preselected genes for a targeted analysis of enzymes involved in these metabolic/epigenetic pathways, it can be considered more highly specific.

The present article is structured as follows. In Part 1, the null hypothesis defined by GIFT will be established. Using Dataset-1 the concept of genetic path pertaining to GIFT will be introduced (Part 2) out of which a p-value for GIFT will be defined (Part 3). Then Dataset-1 (Part 4) and Dataset-2 (Part 5) will be analysed comparing the informational/investigative power of GIFT relative to GWAS using Manhattan plots.

Materials and Methods:

Biological datasets

The first dataset (Dataset-1) analysed 600 pedigree-recorded Scottish Blackface lambs using CT scans to determine *in vivo* carcasses composition (13). The trait selected for the present study is the bone areas of the ischium (BAI) measured in mm^2 from cross-sectional CT scans. The ischium is one of the three bones that make up the pelvis. It is located beneath the ilium and behind the pubis. The upper portion of the ischium forms a major part of the concave portion of the pelvis that forms the hip. As mentioned above this trait was strongly associated with the Chromosome 6 upon using residual phenotypic values. Residual phenotypic values were obtained using an additive model considering the population mean and, as covariates, dam age, year and day of birth, the effect of management group (as sheep were from different farms), sex and litter size. Further information can be found in Matika et al. (2016) (13).

The second dataset (Dataset-2) analysed is new, and comes from a large ongoing programme of research which seeks to identify SNPs that determine individual metabolic and epigenetic responses to nutritionally induced deficiencies in one carbon metabolism (14,15). For this study sheep were used as an experimental model. All animal procedures relating to this study adhered to the Animals (Scientific Procedures) Act, 1986. Associated protocols complied with the ARRIVE guidelines and were approved by the University of Nottingham Animal Welfare and Ethical Review Body (AWERB) with Home-Office project licensed authority (30/3376;10th February 2016).

Dataset-2: Sheep genome re-sequencing, custom array design and SNP profiling of test subjects

Twenty-four unrelated Texel ewes were sequenced to a depth of 30x in 2 pools at Edinburgh Genomics. DNA samples were prepared using Illumina's TruSeq PCR free kits and sequenced on an Illumina HiSeq 2500 Rapid Mode (serial no. D00125), read length of 150PE. Reads were trimmed to remove adapter sequences and low-quality bases using skewer with commands (-Q 20, -q 3) (16) and mapped to the reference sheep genome assembly (Oar_v3.1) using bwa mem (options -M -t 4) (17). Following deduplication using picard-tools version 1.92, variants were called using GATK pipeline (18) including realignment around known indels and recalibration of bases, and FreeBayes (--use-best-n-alleles 4 --pooled-discrete --min-alternate-count 4). Annotation of SNPs was performed using Ensembl variant effect predictor VEP version ensembl tools release 79 (19). 15,347,831 variants were identified. Of these, ~3 million were novel SNPs and ~12 million were already present in the Ensembl genome database. SNPs within annotated coding regions (VEP annotated "downstream gene variant" or "intron variant" removed) and within 3Kb upstream of a gene were retained. SNPs with a minor allele frequency of greater than 0.5 were used to design an Illumina Infinium® iSelect® Custom Array consisting of 4,576 probes. This captured SNPs in 115 1C metabolism and related genes, and 108 related epigenetic regulators as well as 33 control SNPs (Supplementary Material 1).

Liver samples were next collected post-mortem from 360 male and female Texel lambs (6 to 11 months of age) representing 11 farms dispersed regionally across the UK. Collections took place at regional abattoirs and samples immediately snap frozen in liquid N and stored at -80°C until analyses. DNA was then extracted using AllPrep DNA/RNA Mini kit (Qiagen, Manchester UK). Briefly approximately 20 mg of liver were mechanically disrupted using a TissueLyser (Qiagen, Manchester, UK) in 600 RLT plus buffer containing β-mercaptoethanol. Tissue lysates were then used to extract RNA and DNA according to the manufacturer instructions. The custom designed array was then used to SNP profile DNA from these Texel-sheep. For this purpose, liver samples were collected post-mortem from lambs (aged 6 to 11 months) representing 11 farms dispersed regionally across the UK. Collections took place at regional abattoirs and samples immediately snap frozen in liquid N and stored at -80°C until analyses. DNA was then extracted using AllPrep DNA/RNA Mini kit (Qiagen, Manchester UK). Briefly approximately 20 mg of liver were mechanically disrupted using a TissueLyser (Qiagen, Manchester, UK) in 600 RLT plus buffer containing β-mercaptoethanol. Tissue lysates were then used to extract RNA and DNA according to the manufacturer instructions.

Dataset-2: Metabolic profiling

For the purposes of the current study the following seven liver metabolites were selected from a larger pool of 1C metabolites: S-adenosyl methionine (SAM), methylcobalamin (mB12), adenosylcobalamin (aB12), trimethylglycine (TMG), dimethylglycine (DMG), propionate (PPA) and methylmalonic acid (MMA). The first four metabolites were selected as representative intermediates of the methionine cycle whilst the latter two are intermediates in the hepatic synthesis of succinate (15) (Fig.2 & Supplementary Material 1).

Hepatic concentrations of four metabolites (i.e., mB12, aB12, TMG and DMG) were determined by hydrophilic interaction chromatography (HILIC) coupled to electrospray ionization tandem mass spectrometry (MS/MS) as reported previously (20). For the analysis of SAM (determined separately by HILIC), the standard was purchased from Sigma-Aldrich (Poole, Dorset, UK). Stock solutions of this standard were prepared in potassium phosphate extraction buffer (KH_2PO_4 and K_2HPO_4; 40 mmol/L) containing 0.1% L-ascorbic acid, 0.15% citric acid and 0.1% MCE (adjusted to pH 7 with NaOH), each at a final concentration of 100 µmol/L. Also, for SAM the mobile phase was modified from that used for the three other reported metabolites by adjusting the pH of the aqueous ammonium carbonate buffer solution from 3.5 to 9.1. Mass spectrometer parameters for SAM were as follows: retention time = 7.69 min; Q1mass = 399.1 amu; Q3 mass = 250.1 amu; declustering potential = 56; collision energy = 25; collision cell exit potential = 16.

Hepatic concentrations of PPA and MMA were determined by gas chromatography coupled to mass spectroscopic-detection (GC-MS). Briefly, for PPA, 750 µL 5-Sulfosalicylic acid (SSA, 0.04 mg/ml) was added to 150mg frozen liver, homogenised for 2 min and cooled on ice for 10 min. The sample was centrifuged for 15 min at 14,500 x g and 200 µL liver homogenate transferred to a 2.5 mL screw capped glass vial. To this, 20 µL internal standard (MBA, 400 µM), 3.5 µl HCl (37%) and 1 mL diethylether were added, vortexed for 2 min and centrifuged for 10 min at 14,500 x g. 600 µL of the upper layer was transferred to a screw capped glass vial containing 3.5 µL 1-(tert-butyldimethylsilyl)imidazole (TMDMSIM, 97%), vortexed for 2 min and heated at 60°C for 30 min. GC-MS analysis proceeded after cooling. The method used a DB-5MS column (J&W Scientific Agilent technology, 30 m x 0.25 mm; 0.25 µm film thickness). The carrier gas (He) was set at a constant flow rate of 1.3 ml/min. The injection volume was 5 µL for SCAN mode (for qualification) and SIM (selected ion monitoring) mode (for quantification), both using splitless mode. The injection port and MS selective detector interference temperatures were 260°C and 250°C respectively. The chromatograph was programmed for an initial temperature of 40°C for 1 min, increased to 60°C at 70°C min-1, then to 110°C at 15°C min-1, and finally 250°C at 70°C min^{-1}. MS was tuned regularly and operated in electron impact (EI) ionization mode with the ionization energy of 70eV. SCAN mode measured at m/z: 30-300 and SIM ions were set at 159 (for MBA) and 131 (for PPA). The same method was used to produce a calibration curve for PPA using standards at concentrations ranging from 19.5 nmol/g to 5µmol/g. The limit of detection was 19.5 nmol/g. CVs for low, medium and high QCs were 10.4, 6.3 and 6.5% and the inter-assay CV was 4.7%.

For MMA, 250 µL 80% MeOH was added to 50 mg frozen liver, homogenised for 2 min and cooled on ice for 10 min. The sample was ten centrifuged for 15 min at 14,500 x g and 200 µL liver homogenate transferred to a 2.5 mL screw capped glass vial. To this, 4 µL internal standard (1 mM 4-chlorobutyric acid (CBA) in 1 mM HCl) followed by 250 µL 12% BF3-Methanol were added, vortexed for 1 min and heated at 95°C for 15 min. After cooling, 250 µL cold distilled water and 250 µL cold dichloromethane (CH_2Cl_2) were added to the vial, vortexed for 30s and centrifuged for 10 min at 14,500 x g. The lower dichloromethane layer was transferred to a screw capped glass auto-sampler vial with insert for GC-MS analysis. The method used a DB-WAX column (cross-linked polyethylene glycol; J&W Scientific Agilent technology) (30 mm x 0.25 mm; 0.15 µm film thickness). The carrier gas (He) was set at a constant flow rate of 1.0 ml/min. The injection volume was 1 µL for SCAN mode (for qualification) and SIM mode (for quantification), both using splitless mode. The injection port and MS selective detector interference temperatures were 260°C and 280°C respectively. The chromatograph was programmed for an initial temperature of 50°C for 2 min, increasing to 150°C at 8°C min-1, then to 220°C at 100°C min^{-1} and held for 5 min at the final temperature. MS was tuned regularly and operated in EI ionization mode with the ionization energy of 70eV. The limit of detection was 0.75 nmol/g for both MMA and SA and inter-assay CVs were 8.4% for MMA and 11.0% for SA.

Dataset-2: Determination of GWAS for 1C-metabolites

Several statistical models were tested to adjust phenotypic values of 1C-metabolites and it was found that the most informative model was a linear univariate model once phenotypic data were log-transformed using the natural logarithm (Supplementary Material 2). Transformed data were then pre-corrected for the fixed effects of farm (F) and sex (S) in ASReml using the following model, $y_{ij} = \mu + F_i + S_j + e_{ij}$, where y_{ij} is the log-transformed phenotype, that is the log-transformed metabolite concentration studied; μ is the overall mean for the log-transformed metabolite concentration; F_i is the effect of the ith farm (i =1,..,11); S_j the effect of jth Sex (Male vs Female) and, e_{ij} is the residual error that was used to extract genotype-phenotype mapping information. The genotype dataset was filtered using PLINK (HWE p-value threshold of 10^{-6}, call rate for genotypes of 10% and a MAF of 5%), the number of independent SNPs was determined using BCFTOOLS (r^2-threshold=0.1) and the GWAS Manhattan plots, linked to the determination of p_{GWAS}, were obtained using GEMMA. The same genotype and residual phenotypes as filtered by GWAS were used by GIFT.

Data representation using GIFT and related significance.

Adjusted phenotypic data (i.e., residuals, from Dataset-1 and Dataset-2) were used for this study. Regarding the representation of GIFT, upon selecting a SNP for all individuals, the different corresponding genotypes, aa, aA/Aa and AA, were assigned the arbitrary values +1, 0 and -1, respectively. With this convention any barcode can be represented by a string of numbers from which a GIFT analysis can be inferred. More specifically, the assignment of values +1, 0 and -1 were done as a function of the base pairs as follow: AA=TT=+1, GG=CC=-1 and 0 otherwise. As shown schematically in Fig.1, the residuals obtained were ranked by order of magnitude and the cumulative sum of their corresponding genotypic values performed to obtain the 'genetic path' for the SNP considered. The genetic path of a SNP is noted $\theta(i)$ in the text (Fig.1).
The null hypothesis $\theta_0(i)$ for the SNP considered can be obtained by scrambling (a.k.a. permutation test) the string of microstates represented in Fig.1A (bottom), which is equivalent to losing the information accrued initially on phenotypic values. Repeating the scrambling an infinite number of times, and plotting the average scrambled genetic path, returns a straight line of the form, $\theta_0(j) = (+1 \cdot N_+/N + 0 \cdot N_0/N - 1 \cdot N_-/N)i$. This result comes from the fact that, when scrambling an infinite number of times, the microstates in the string Fig.1A (bottom) is equivalent to determining, for any position i, the presence probability of each microstate in the string. Consequently, each SNP has its own null hypothesis that is a function of the number and type of microstates defining the SNP studied across the population.
The p-value for GIFT was determined as explained in the text (a full part is dedicated to it) under the condition that the microstates composing the SNP were such that the minimum number of microstates of one type was at least 3. The rationale behind this condition is linked to the fact that, mathematically, n!, can be approximated by Stirling formula, $n! = \sqrt{2\pi n}n^n e^{-n}$, if $n \geq 3$, which is reasonably accurate for n as low as 3.

Results and discussion

Analyse of the null hypothesis $\theta_0(i)$ for GIFT

While $\theta(i)$ is obtained using phenotypic information (Fig.1), it is also possible to plot the cumulative sum of microstates when no phenotypic information is present that is equivalent to 'scrambling' or permutating the string of microstates in Fig.1A also corresponding to the configuration ② in Fig.1B. Recall that since our focus is on a given SNP, then the number of microstates, N_+, N_0 and N_-, are identical between the configurations ① and ②. This new cumulative sum noted $\theta_0(i)$ is expected to be a sort of null hypothesis solely dependent on the bulk microstate frequencies N_+/N, N_0/N and N_-/N, where N_q $q \in \{+,0,-\}$ is the number of microstates of type q. This is so because there is no further information that could inform on the positioning of microstates in their list when the scrambled state is considered. However, while $\theta(i)$ is unique since phenotypic information is used to generate it, $\theta_0(i)$ is not as each time the string of microstates from Fig.1A is scrambled, a new $\theta_0(i)$ appears. Accordingly, one needs to consider the set of possible $\theta_0(i)$s generated bounded to the microstate frequencies N_+/N, N_0/N and N_-/N.

Using a selection of theoretic SNPs defined by different microstate frequencies (Table-1). Fig.3A illustrates the global shape resulting from simulating 1000 $\theta_0(i)$s. The results demonstrate that the global shape of the $\theta_0(i)$s plotted as a function of the position in the string is ellipsoidal with short and long axes changing as a function of microstate frequencies involved, and where the different averages of $\theta_0(i)$s represented by black lines in Fig.3A, are straight lines with slopes linked to the difference, $\Delta N/N = (N_+ - N_-)/N$. The fact that the averages of $\theta_0(i)$s for a given set of microstates, N_+, N_0 and N_-, is always a straight line linked to microstate frequencies, N_+/N, N_0/N and N_-/N, can be understood intuitively by the fact that scrambling or permutating an infinite number of times the string of microstates is equivalent to determining, for any position i, the presence probability, N_q/N, of each microstate in the string. Accordingly, for a given set of microstates, N_+, N_0 and N_-, the average of $\theta_0(i)$s, noted $\langle\theta_0(i)\rangle$, is $\langle\theta_0(i)\rangle = \frac{(N_+ - N_-)}{N} i$. Further theoretic details can be found in (10,11). Using $\langle\theta_0(i)\rangle$ as a reference for the null hypothesis, Fig.3B show the sur-imposition of the differences, $\Delta\theta_0(i) = \theta_0(i) - \langle\theta_0(i)\rangle$, obtained from simulations using SNPs from Table-1.

Finally, to assess the impact of the sample size (population size) on the null hypothesis the initial size (N=565, Table-1) was divided (N=280) and multiplied (N=1130) by a factor ~2 while keeping constant the microstate frequencies N_+/N, N_0/N and N_-/N from Table-1. The simulations Fig.3A show that the appearance of ellipsoids is affected when the sample size changes, becoming thinner as the population size increases. Plotting the standard deviation as a function of the position once normalised by the sample size, $\sigma(i/N) = \sqrt{\left[\langle(\theta_0(i/N))^2\rangle - \langle\theta_0(i/N)\rangle^2\right]/N}$, resulting from the different simulations in Fig.3C demonstrates that the standard deviation from GIFT is quadratic, and independent of the sample size, as expected from a random allocation of different microstates in the string of positions.

At first sight and with this primary analysis one could suggest that any genetic path departing from the cloud of genetic paths formed by the set of $\theta_0(i)$s upon the permutation of microstates (grey surface in Fig.3A or black surface in Fig.3B) would likely result in an association between the genotype and the phenotype. While true this assumption needs to be handed carefully as it is not exhaustive. Indeed, some genetic paths may be highly structured and of relatively small amplitude. Example of genetic paths using real data from Dataset-1 will demonstrate this point.

Examples of genetic path using the bone area of the ischium (BAI) as phenotype (Dataset-1)

The resulting average, $\langle\theta_0(i)\rangle$, and variance, $\sigma(i)$, can be used to inform the null hypothesis of a particular SNP from 'real' datasets. However, since there are as many different sets of $\theta_0(i)$s as number of SNPs, each SNP will return its own $\langle\theta_0(i)\rangle$ (null hypothesis) upon scrambling. A comparison between SNPs using GIFT/genetic paths requires then to concentrate on the differences, $\Delta\theta(i) = \theta(i) - \langle\theta_0(i)\rangle$. In the remaining text one shall rewrite $\langle\theta_0(i)\rangle$ as $\theta_0(i)$ to simplify notations.

Concentrating now on 'real' dataset, the genetic paths were obtained further to ranking BAI residual values (Dataset 1) using an incremental rank from small to large values. As an example, Fig.4 shows the two genetic paths $\theta(\mathrm{i})$ and $\theta_0(\mathrm{i})$ for six SNPs, renamed SNP1-6 (see Table-2 for accurate genetic information) enabling us to appreciate the qualitative difference between the genetic paths. While the null hypothesis, i.e., $\theta_0(\mathrm{i})$, resulting from the scrambling of phenotypic values many times always returns a straight line with a different slope for each SNP as seen above, the $\theta(\mathrm{i})$s have different shape. To represent the set of $\theta(\mathrm{i})$s in relation to the different microstates involved, each datapoint of the $\theta(\mathrm{i})$s is colour coded as in Fig.1C.

Since $\theta_0(\mathrm{i})$ is linked to the difference between the genetic microstate frequencies of homozygotes, $\Delta\mathrm{N} = \mathrm{N}_+ - \mathrm{N}_-$, in Fig.4 we represent by the angle α such difference. Since $\tan(\alpha) = +\mathrm{N}_+/\mathrm{N} - \mathrm{N}_-/\mathrm{N}$ where N is the total number of positions $(\mathrm{i} = 1, 2, \ldots, \mathrm{N})$ $\theta_0(\mathrm{i})$ can be rewritten as, $\theta_0(\mathrm{i}) = \tan(\alpha)\mathrm{i}$. As any analysis must concentrate on the difference, $\Delta\theta(\mathrm{i}) = \theta(\mathrm{i}) - \theta_0(\mathrm{i})$, such as to cancel the apparent variability in the null hypothesis across SNPs, we represent the plots of the different $\Delta\theta(\mathrm{i})$s obtained in the right panel of Figs.4A-4F.

Figs.4A-4B display two distinct genetic paths that are globally similar. While they have different number of microstates of each type (see Table-2) the $\Delta\theta(\mathrm{i})$s of SNP1 and SNP2 are characterised by their small amplitudes and the fact that they are erratic crossing several times the axis of position corresponding to the null hypothesis. In those cases, using the information contained in the phenotypic residuals, namely ranking the phenotypic residuals from small to large values, does not permit to fully differentiate $\theta(\mathrm{i})$ from $\theta_0(\mathrm{i})$. On the other hand, the right panel in Figs.4C-4D for SNP3 and SNP4 demonstrates, in a more noticeable way, a paraboloid shape for the $\Delta\theta(\mathrm{i})$s resulting from a segregation of microstates upon ordering the phenotypic residuals. The segregation of microstates +1 and -1 in opposite direction is reminiscent of Fisher theoretic works (Fig.1). As it turns out Figs.4C-4D show some similarities with Fig.1C based on a simulation inspired by Fisher's seminal works. Importantly the $\Delta\mathrm{N}$-values of SNP1 and SNP4 while of opposite sign are similar in absolute value, are as those of SNP2 and SNP3, suggesting, in turn, the $\Delta\mathrm{N}$-values do not impact on the ability to differentiate $\theta(\mathrm{i})$ from $\theta_0(\mathrm{i})$. Namely that a segregation of microstates can be inferred also with relatively large and opposed $\Delta\mathrm{N}$-values.

Envisaging the migration of microstates +1 and -1 in opposite direction as initially postulated by Fisher as the sole framework to associate genotype and phenotype is not always valid. This is demonstrated by SNP5 and SNP6 and the appearance of structured genetic paths displaying clear sigmoidal shapes for the $\Delta\theta(\mathrm{i})$s as shown in Figs.4E-4F. Theoretically this phenomenon can be understood and explained by the presence of non-linear phenotypic fields, see (11) also reviewed in (12), in turn breaking the symmetry postulated by Fisher assuming the sole presence of linear phenotypic fields. This type of sigmoidal shapes is of interest since they inform on potential regulation mechanisms involving very probably 'regulatory variants' (21). Indeed, the right panels in Figs.4E-4F can be envisioned as representing the genetic organisation of two distinct subpopulations of phenotypic residual values, one above the dashed line and the other one underneath it. Taken separately those two subpopulations draw curves like Figs.4C-4D or Fig.1C. In this context it is tempting to suggest that sigmoid genetic paths reveal a type of genotype-phenotype association that is inherently 'scale-dependent', namely function of the magnitude of phenotypic residuals. Because traditional GWAS concentrates on averages and variances, these sigmoid paths would be remarkably difficult to characterise with traditional methods. This is so because there is no clear antisymmetric segregation of microstates. As an example, using SNPs1-6 (from Fig.4) we have plotted, in Fig.5, the average values of phenotypic residuals for each microstate, and in Table-2 we provide the resulting gene/size effects and the dominances associated with those. Fig.5 and Table-2 demonstrate that sigmoid genetic paths (SNP5 and SNP6) are much less detectable with traditional methods while paraboloid genetic paths (SNP3 and SNP4) are. Note that the numerical determination of '$-\mathrm{Log}_{10}(\mathrm{p}_{\mathrm{GIFT}})$' in Table-2, that is the significance for GIFT, is explained in the next part below.

To conclude, based on Fisher's theoretic works, traditional GWAS method has been optimised to map SNPs that, using GIFT, would draw paraboloid genetic paths (see Fig.1C). The potential novelty using GIFT resides in its ability to provide new information and detect relatively regular/structured sigmoid genetic paths that would otherwise not be detected by traditional methods.

p_{GIFT}: p-value for GIFT

GIFT and GWAS extract information on genotype-phenotype associations in totally different ways. While GIFT concentrates on the significance of curves drawn using $\Delta\theta(i) = \theta(i) - \theta_0(i)$, GWAS focuses solely on the significance of difference of averages. However, to compare GIFT to GWAS it is essential to determine a p-value for GIFT that is exhaustive enough such as to also capture the information that GWAS provides. To this end a p-value was derived that concentrates on the maximal amplitudes difference of genetic paths (see Figs.6A-6B).

The p-value for GIFT can be understood as follows. Since the number of possible paths is linked to the number of configuration possible resulting from lodging N_+, N_0 and N_- microstates into a list composed of $N = N_+ + N_0 + N_-$ components, the number of possible paths is, $N^0_{path} = \frac{N!}{N_+!N_0!N_-!}$. Let us now divide the genetic paths into regions, Δi_1, Δi_2 and Δi_3 as shown in Figs.6A-6B. As the number of microstates of each sort can be determined in each region using an adequate algorithm, then the total number of possible genetic paths in this first, second and third regions are, respectively, $N_1 = \frac{\Delta i_1!}{(n_+)_1!(n_0)_1!(n_-)_1!}$, $N_2 = \frac{\Delta i_2!}{(n_+)_2!(n_0)_2!(n_-)_2!}$ and, $N_3 = \frac{\Delta i_3!}{(n_+)_3!(n_0)_3!(n_-)_3!}$, where $\left(n_q\right)_p$ is the number of microstate of type q in the p^th^ region, $q \in \{+,0,-\}$ and $p \in \{1,2,3\}$. Consequently, the probability of a genetic path in this context is, $p_{GIFT} = N_1N_2N_3/N^0_{path}$. Using the null hypothesis simulations shown in Fig.3 based on the theoretic SNPs given in Table-1, p_{GIFT} may be determined for each genetic path simulated. Its statistic plotted in Fig.6C for each SNP demonstrates very little variations across SNPs or when the sample size change by a factor two. Based on this observation confidence intervals were determined for all SNPs by averaging the p_{GIFT} values obtained. The upper and lower red dashed lines represent the 99% and 95% confidence intervals. Returning to Table-2 the numerical value of p_{GIFT} was determined for the genetic paths shown in Fig.4 demonstrating that GIFT can extract information when sigmoid genetic paths are involved while traditional GWAS is unable to do so.

Armed with p_{GIFT} an analysis of datasets can now be performed.

Comparison between GWAS and GIFT considering the bone area of the ischium (BAI) as phenotype (Dataset-1)

The first dataset (Dataset-1) analysed 567 pedigree-recorded Scottish Blackface lambs concentrating on the bone areas of the ischium measured in mm^2 from cross-sectional CT scans (13). After adjusting phenotypic values, the work demonstrated a clear involvement of chromosome 6 as shown in Fig.7A. The thresholds applied for GWAS in Fig.7A correspond to 99% (upper red dashed line) and 95% confidence intervals (lower dashed red line) determined by using independent SNPs only. Formally a 99% (resp. 95%) confidence interval is given by, $-\text{Log}_{10}\left((1-99\%)/N_{ind-SNPs}\right)$ (resp. $-\text{Log}_{10}\left((1-95\%)/N_{ind-SNPs}\right)$ where $N_{ind-SNPs} = 10433$ is the number of independent SNPs. Using its own thresholds (Fig.6C) GIFT was applied using the same set of phenotypic residuals. Figs.7A-7B demonstrate the results obtained by GWAS and GIFT using Manhattan plots. Overall, there is an agreement between GWAS and GIFT that chromosome 6 is involved. However, differences exist that are shown through the involvement of several chromosomes when GIFT is used. Considering the thresholds involved, for GWAS the phenotype studied may be considered as a sort of ‘single gene trait’ while for GIFT, the phenotype looks very much like a ‘complex trait’ involving more chromosomes than the chromosome 6. A detailed information of all significant SNPs by GWAS or GIFT is given in Supplementary Material 3).

Concentrating on Chromosome 6 to address the overlap of information provided by GIFT and GWAS, a Venn-diagram including highly significant SNPs only, namely SNPs beyond the upper red dashed-line representing the 99% confidence interval in Figs.7A-7B, was plotted. The Venn-diagram (Fig.7C) reveals that most SNPs deemed significant by GWAS were also deemed significant by GIFT. Curiously, only one SNP seemed highly significant by GWAS but irrelevant for GIFT. As p_{GIFT} was designed to collect exhaustive information from GWAS, the SNP was identified (OAR6_40311379) and its genetic path, i.e., its $\Delta\theta(i)$, plotted (Fig.7D-left) together with its GWAS-representation (Fig.7D-right). The genetic path, being erratic of relatively small amplitude and crossing several times the axis of positions, did not display any obvious ‘parabolic or sigmoidal’ associations at first sight, in turn justifying its small p_{GIFT}-value. The GWAS-representation of OAR6_40311379 however, demonstrated the absence of microstate '-1' as well as a near overlap of the means for the microstates '0' and '+1' suggesting the occurrence of a false-positive. To confirm this a comparison of phenotypic means for the microstates '0' and '+1' was performed returning a t-test value of 1.1485 (p-value of 0.2512), confirming the presence of a false-positive.

As SNPs were selected based on a 99%-interval confidence, to confirm that OAR6_40311379 corresponds to the 1%-aberration we plotted in Fig.7E the first 100 more significant SNPs detected by GIFT and GWAS. Results confirm an overlap of SNPs associated with the phenotypic residuals for large values of p_{GIFT} and p_{GWAS} (see purple dots in Q_2 in Fig.7E). Interestingly, two SNPs considered as significant by GWAS (two blue dots in Q_2) were not by GIFT. That is because the p_{GIFT}-values for these dots were less than other SNPs detected by GIFT. As already stated above many SNPs from other chromosomes were considered significant by GIFT that were not by GWAS (see red dots in Q_4). Finally, the quadrant Q_1 in Fig.7E confirms that OAR6_40311379 is a standalone SNP among the 100 SNPs (1%) since it is the only SNP for which $p_{GWAS} > p_{GIFT}$, confirming its false-positive or 1%-aberration status.

The biotype of significant SNPs on Chromosome 6 for GIFT and GWAS are also presented in Fig.7F.

The primary conclusion provided by Fig.7 is that, when compared to GWAS, GIFT returns substantially more genetic information. At present, we do not know how the whole information provided by GIFT may inform on the putative biology of the phenotype studied (BAI). As it turns out, a full validation of the information provided by GIFT on Dataset-1 would require an in-depth mutational/deletion/insertion/gene-editing analyses in live animals, extending beyond the scope of this present article.

Instead of revisiting the genetic basis of BAI, to demonstrate the relevance of the information provided by GIFT we decided to challenge GIFT using a different dataset (Dataset-2) concentrating on a complex trait related to 1C-metabolism.

Comparison between GWAS and GIFT considering 1C-metabolites as phenotype (Dataset-2)

Dataset-2 concerns biochemical data which seeks to identify risk allele variants in genes whose products direct a specific series of metabolic pathways, known as one carbon (1C) metabolism (Fig.2). The significance of 1C metabolism is that it is a complex trait involving a series of interlinking metabolic pathways that provide 1C units (methyl groups) for the synthesis and methylation of biological molecules. In Fig.8A the Manhattan plots obtained by GWAS and GIFT are shown clearly demonstrating that the informational power of GWAS is less than that of GIFT. Note that the number of independent SNPs, in this case is 624 (out of 3923 SNPs inputted in the gene array). Finally, in Fig.8B we provide the biotypes of the most significant SNPs, namely those above the 99% confidence interval shown by the upper red dashed lines obtained using GIFT. Detailed genetic information of the most significant SNPs obtained using GIFT is provided in Supplementary Material 4.

Besides validating that the information extracted by GIFT is meaningful, in turn positioning GIFT as a new method to map genotype to phenotype, it is worth underlying the biological importance and novelty of results obtained. One carbon metabolism in sheep is comparable to that in humans. The significance of 1C metabolism is that it is a complex trait involving a series of interlinking metabolic pathways that provide 1C units (methyl groups) for the synthesis and methylation of chromatin among other molecules (15). S-adenosylmethionine (SAM) is a potent methyl donor within these cycles and serves as the principal substrate for methylation of DNA, associated proteins, and RNA. It was previously demonstrated in sheep, cattle, rodent and human studies that disrupting these cycles during early pregnancy, by either dietary means (i.e., reducing dietary vitamin B12, folate, choline and/or methionine), or through exposure to environmental chemicals such as cigarette smoking, can lead to epigenetic dysregulation and impaired foetal development with long-term consequences for offspring cardiometabolic health (22–25). It was also advocated that interindividual and ethnic variability in epigenetic gene regulation arises because of single-nucleotide polymorphisms (SNPs) within 1C genes, associated epigenetic regulators, and differentially methylated target DNA sequences (15). However, information concerning the nature and extent of interactions between parental genotype, diet and EC exposure was, until now, limited to just a few 1C genes in humans (15). Consequently, data obtained by the current study provide new evidence concerning significant genetic variants in 1C-metabolism and directly associated metabolic genes and epigenetic regulators that rely on SAM as the methyl donor, potentially applicable to the human species.

Concluding remarks

While statistical association methods should not favour any biases when analysing datasets, the way they are built mathematically is often indicative of a particular way of thinking. For example, with GWAS the phenotype is decomposed onto more fundamental sub-distributions characterised by the distribution of microstates (see Fig.1A). This approach underlines a sort of bottom-up approach that, within a reductionist framework, defines genes as biological agents controlling the phenotype aligned with the 'Neo-Darwinian synthesis'. However, nothing prevents considering the opposite as far as statistical association methods are involved, and GIFT uses this degree of freedom. By using the full range of phenotypic information, GIFT transforms a random or disordered string of microstates (the straight line in the asymptotic limit seen in Fig.1C or Fig.3A) into an 'ordered' configuration of microstates (see Fig1C or Figs.4C-4F), in turn providing the signature of a genotype-phenotype association. Accordingly, since the phenotypic information controls the configuration of microstates it is a top-down approach, which turns out to be remarkably sensitive. GIFT has been estimated to be ~1000 more sensitive than GWAS (11).

There are three main reasons as to why GIFT is more sensitive. The first is that GIFT determines the significance of curves composed of an entire population of datapoints. As curves provide greater level of significance than considering differences between microstate/phenotypic averages/variances as advocated by GWAS, hence GIFT is statistically more powerful. The second reason is that the null hypothesis for GIFT, namely $\theta_0(i)$, is contained in the definition of $\Delta\theta(i)$ and is therefore specific to the genome position, or SNP, studied. With GIFT there are as many null hypotheses as SNPs. This contrasts with GWAS defining a null-hypothesis valid for all SNPs at the population level when the average of microstate distributions overlap. Consequently, the discriminative power of GIFT is amplified. The third reason is that GIFT is simpler than GWAS. Indeed, based on R.A. Fisher's seminal work, GWAS is based on a complex theory that seeks to determine genotype-phenotype associations on one hand (aim 1), and the heritability of phenotypes/traits studied on the other (aim 2). To achieve those two aims, the GWAS approach relies on frequentist probability to determine the validity of statistical inferences giving the notions of average and variance fundamental meanings related to aim 1 and 2, respectively. However, because average and variance are antinomic it is nearly impossible to have a clear picture of associations (size effects) since the noise (variance/heredity) blurs the average(s). On the opposite, by concentrating on genetic paths (curves) GIFT determines a global association. This does not mean that GIFT rules out the notions of size effect, dominance, and heritability, on the contrary, it encapsulates them under the generic notion of phenotypic field, i.e., size effect, dominance and heritability can be rederived from the phenotypic field. The term 'field' in the acronym GIFT is used to explain the disorder-order transition in the string of microstates using an analogy related to physics field theory, see (11,12) for more details.

Finally, it is important to reframe GIFT within current debates in the field of biology. With GIFT it is the (information on the) phenotype that selects which SNP is required for its subsistence and it is interesting to note that, at the conceptual level and as a top-down approach, GIFT has some familiarity with the notion of phenotypic plasticity. Phenotypic plasticity refers to the ability of phenotypes to respond to a change in the environment favouring a divergence from the ancestor phenotype. As the phenotype relies on traits (modules), the responsiveness to any new input(s) must involve a re-organisation of the phenotype architecture by allowing phenotypic sub-components (modular traits) to adapt the changes (26). Namely that genetic accommodation linked to a standing pool of genetic variations characterising any trait is central to phenotypic plasticity that, through persistence, may genetically assimilate the new architecture (selection) (26,27). In this context the top-down method GIFT, which is essentially a phenotype-genotype (and not genotype-phenotype) association method, can pull out any standing genes awaiting to be used by phenotypes.

To conclude, we provide evidence that GIFT is more powerful than GWAS in determining potential associations between continuous (phenotypes) and discontinuous (microstates) datasets. Additionally, we provide evidence also for the need to rethink the conceptual bases of genotype-phenotype associations, especially those giving too strong biological meanings to a bottom-up approach, such as to go beyond the notions of average, variance and use more information from the whole biodiversity of data.

Acknowledgements: This work was supported by the Biotechnology and Biological Sciences Research Council (BBSRC) Industrial Partnership Award with the Agriculture and Horticulture Development Board, Meat Promotion Wales and Agrisearch [BB/K017810/1; BB/K017993/1], and National Institutes of Health (R01 ES030374/ES/NIEHS NIH HHS/United States). P.K. is currently supported by a Doctoral Scholarship from the EPHE, Sorbonne University in collaboration with the University of Nottingham. C.E.C. was in receipt of a BBSRC Doctoral Training Partnership scholarship (1796056) and A.H.B. was in receipt of a scholarship from The Perry Foundation. The authors would like to thank Dr Barbara Bravi, Dr Wing-Yee Kwong and Dr Dongfang Li for useful discussions and/or technical assistance.

Contributions: CR conceptualised GIFT; CR & JW formalised GIFT; PK coded GIFT simulations; Dataset-2 was designed and obtained by KDS, OM, AHB, CEC, JX, DAB, RDE; Dataset-1 and Dataset-2 were analysed by PK, CR, JW, KDS, OM, AP; paper was written by CR and KDS, and proofread by CR and KDS.

Declaration: The authors declare no competing interests.

References

1. Burton PR, Clayton DG, Cardon LR, Craddock N, Deloukas P, Duncanson A, et al. Genome-wide association study of 14,000 cases of seven common diseases and 3,000 shared controls. Nature. 2007 Jun 1;447(7145):661–78.

2. Buniello A, MacArthur JAL, Cerezo M, Harris LW, Hayhurst J, Malangone C, et al. The NHGRI-EBI GWAS Catalog of published genome-wide association studies, targeted arrays and summary statistics 2019. Nucleic Acids Res. 2019 Jan 8;47(D1):D1005–12.

3. Sudlow C, Gallacher J, Allen N, Beral V, Burton P, Danesh J, et al. UK biobank: an open access resource for identifying the causes of a wide range of complex diseases of middle and old age. PLoS Med. 2015 Mar;12(3):e1001779.

4. Smith BH, Campbell A, Linksted P, Fitzpatrick B, Jackson C, Kerr SM, et al. Cohort Profile: Generation Scotland: Scottish Family Health Study (GS:SFHS). The study, its participants and their potential for genetic research on health and illness. Int J Epidemiol. 2013 Jun;42(3):689–700.

5. Fisher RA. XXI.—On the Dominance Ratio. Proc R Soc Edinb. 1923;42:321–41.

6. Fisher RA. XV.—The Correlation between Relatives on the Supposition of Mendelian Inheritance. Trans R Soc Edinb. 1919;52(2):399–433.

7. Visscher PM, Goddard ME. From R.A. Fisher's 1918 Paper to GWAS a Century Later. Genetics. 2019 Apr;211(4):1125–30.

8. Hivert V, Wray NR, Visscher PM. Gene action, genetic variation, and GWAS: A user-friendly web tool. PLoS Genet. 2021 May;17(5):e1009548.

9. Nelson RM, Pettersson ME, Carlborg Ö. A century after Fisher: time for a new paradigm in quantitative genetics. Trends Genet TIG. 2013 Dec;29(12):669–76.

10. Wattis JAD, Bray SM, Kyratzi P, Rauch C. Analysis of phenotype-genotype associations using genomic informational field theory (GIFT). J Theor Biol. 2022 Sep 7;548:111198.

11. Rauch C, Kyratzi P, Blott S, Bray S, Wattis J. GIFT: new method for the genetic analysis of small gene effects involving small sample sizes. Phys Biol. 2022 Nov 3;20(1).

12. Rauch C, Wattis J, Bray S. On the Meaning of Averages in Genome-wide Association Studies: What Should Come Next? Org J Biol Sci. 2023 Jan;6(1):7–22.

13. Matika O, Riggio V, Anselme-Moizan M, Law AS, Pong-Wong R, Archibald AL, et al. Genome-wide association reveals QTL for growth, bone and in vivo carcass traits as assessed by computed tomography in Scottish Blackface lambs. Genet Sel Evol GSE. 2016 Feb 8;48:11.

14. Clare CE, Pestinger V, Kwong WY, Tutt DAR, Xu J, Byrne HM, et al. Interspecific Variation in One-Carbon Metabolism within the Ovarian Follicle, Oocyte, and Preimplantation Embryo: Consequences for Epigenetic Programming of DNA Methylation. Int J Mol Sci. 2021 Feb 12;22(4).

15. Clare CE, Brassington AH, Kwong WY, Sinclair KD. One-Carbon Metabolism: Linking Nutritional Biochemistry to Epigenetic Programming of Long-Term Development. Annu Rev Anim Biosci. 2019 Feb 15;7:263–87.

16. Jiang H, Lei R, Ding SW, Zhu S. Skewer: a fast and accurate adapter trimmer for next-generation sequencing paired-end reads. BMC Bioinformatics. 2014 Jun 12;15:182.

17. Li H, Durbin R. Fast and accurate short read alignment with Burrows-Wheeler transform. Bioinforma Oxf Engl. 2009 Jul 15;25(14):1754–60.

18. Van der Auwera GA, Carneiro MO, Hartl C, Poplin R, Del Angel G, Levy-Moonshine A, et al. From FastQ data to high confidence variant calls: the Genome Analysis Toolkit best practices pipeline. Curr Protoc Bioinforma. 2013;43(1110):11.10.1-11.10.33.

19. McLaren W, Gil L, Hunt SE, Riat HS, Ritchie GRS, Thormann A, et al. The Ensembl Variant Effect Predictor. Genome Biol. 2016 Jun 6;17(1):122.

20. Xu J, Clare CE, Brassington AH, Sinclair KD, Barrett DA. Comprehensive and quantitative profiling of B vitamins and related compounds in the mammalian liver. J Chromatogr B Analyt Technol Biomed Life Sci. 2020 Jan 1;1136:121884.

21. Boyle EA, Li YI, Pritchard JK. An Expanded View of Complex Traits: From Polygenic to Omnigenic. Cell. 2017 Jun 15;169(7):1177–86.

22. Maloney CA, Hay SM, Young LE, Sinclair KD, Rees WD. A methyl-deficient diet fed to rat dams during the peri-conception period programs glucose homeostasis in adult male but not female offspring. J Nutr. 2011 Jan;141(1):95–100.

23. Sinclair KD, Allegrucci C, Singh R, Gardner DS, Sebastian S, Bispham J, et al. DNA methylation, insulin resistance, and blood pressure in offspring determined by maternal periconceptional B vitamin and methionine status. Proc Natl Acad Sci U S A. 2007 Dec 4;104(49):19351–6.

24. Drake AJ, O'Shaughnessy PJ, Bhattacharya S, Monteiro A, Kerrigan D, Goetz S, et al. In utero exposure to cigarette chemicals induces sex-specific disruption of one-carbon metabolism and DNA methylation in the human fetal liver. BMC Med. 2015 Jan 29;13:18.

25. Rubini E, Snoek KM, Schoenmakers S, Willemsen SP, Sinclair KD, Rousian M, et al. First Trimester Maternal Homocysteine and Embryonic and Fetal Growth: The Rotterdam Periconception Cohort. Nutrients. 2022 Mar 8;14(6).

26. West-Eberhard MJ. Developmental plasticity and the origin of species differences. Proc Natl Acad Sci U S A. 2005 May 3;102 Suppl 1(Suppl 1):6543–9.

27. Palmer AR. Symmetry Breaking and the Evolution of Development. Science. 2004;306(5697):828–33.

Table 1: Theoretics SNPs used to capture the null hypothesis associated with GIFT upon 1000 simulations of microstates permutation*.

SNP NAME	N_+	N_0	N_-	N
SNP1	25	25	515	565
SNP2	25	125	415	565
SNP3	25	225	315	565
SNP4	25	325	215	565
SNP5	25	425	115	565
SNP6	25	525	15	565

(*): The difference between consecutive SNPs in the table is linked to the transfer of 100 microstates from the microstates '-1' to the microstate '0' leaving the number of microstates '+' invariant. By permutating the microstates '+' and '-' in the table similar plots as those obtained in Fig.3A could have been obtained, the only difference would have been the slopes of the average $\langle \theta_0(i) \rangle$ changing sign.

Table 2: Determination of gene/size effect (a) and dominance (d) for SNP1-6 from dataset-1. The level of significance for GIFT and GWAS is colour coded: red=not-significant, green=significant.

CHR	NAME	POSITION	$-\text{Log}_{10}(p_{GIFT})$	$-\text{Log}_{10}(p_{GWAS})$	N_+	N_0	N_-	a*	d**
9	OAR9_58767921 (**SNP1**)	56039025	2.844431	0.273539479	391	160	16	N/A	N/A
3	s02120 (**SNP2**)	213625709	2.950364	0.001827486	198	291	78	N/A	N/A
6	OAR6_40855809 (**SNP3**)	36655091	33.11563	9.8639336	229	262	76	96.85	-13.01
6	OAR6_38315830 (**SNP4**)	34256151	24.58108	3.7366937	24	222	321	-70.02	-0.05
23	OAR23_35510473 (**SNP5**)	33556377	23.48392	0.2301613	254	260	53	N/A	N/A
25	OAR25_30372586 (**SNP6**)	29046746	22.10658	1.0692863	90	266	211	N/A	N/A

(a*): The gene/size effect is calculated considering the mid-distance between the average values of phenotypic residuals of microstates '-1' and '+1'. (d**): The dominance is calculated considering the difference between the gene/size effect (a) and the position of the average value of phenotypic residuals for the microstate '0'.

Legends

Figure 1: **(A)** For diploid organisms and for a binary (bi-allelic, A or a) genetic marker, any microstate (genotype) can only take three values that we shall write as '+1', '0' and '-1' corresponding to genotypes aa, Aa and AA, respectively. The genotypes are color-coded to facilitate the representation of GIFT (+1:aa (red), 0: aA/Aa (black) and -1:AA (blue)). GWASs rely on probability density functions formed through the grouping of data into bins/categories. The phenotype distribution density function (A-top left) is then decomposed onto the distribution density function of genetic microstates (A-top right) for every single nucleotide polymophism (SNP). Using an analysis of averages and variances such decomposition determines whether the SNP studied is associated with the phenotype by comparing the average and variances of distributions. Repeating the same operation for every SNP in the genome permits to map genotype to phenotype. However, as more precise inferences can only come with, and are only legitimized by, a reduction in the width of categories, larger sample sizes are needed. To overcome this issue one way to proceed is to deconstruct density functions and wonder what would happen if one were able to reduce the width of categories, that is increasing the precision in the measurement of the phenotype or equivalently getting access to the whole information the datasets, without changing the sample sizes (**A** from top-to-bottom). The mathematical object that emerges is then a coloured barcode that is a list of microstates that can be analysed precisely by GIFT. **(B)** Such barcode can be obtained simply at the practical level through field studies. Assume a flock of sheep has been genotyped and that their phenotype has been measured sufficiently precisely such as to exclude the possibility that any two phenotypic values are identical. In the figure the magnitude of the phenotypic value for each sheep is characterised by the (unique) 'size' of the sheep. The barcode is obtained by ranking animals as a function of the magnitude of their phenotypic values (configuration ①in Fig.1B). The null hypothesis is obtained via the random ranking of sheep that is equivalent to a lack of information on phenotypic values (configuration ② in Fig.1B). As GWAS works on phenotypic residual values after adjusting for fixed/environmental effects a similar barcode can be generated considering the magnitude of residual phenotypic values. **(C)** GIFT proceeds by plotting the cumulative sum of microstates as a function of the position in the list generating a curve called genetic path that is represented by $\theta(i)$ in Fig.1C and is unique to the SNP considered. While the curve $\theta(i)$ does not provide any significant information on its own, one may generate, for the same SNP, a curve (genetic path) corresponding to a sort of null hypothesis when ranking the phenotype does not bring any informational value. This is possible by scrambling (permutating) the string of microstates an infinite number of times. It is then possible to show that, in the asymptotic limit, the null hypothesis returns a straight line, noted $\theta_0(i)$ (Fig.1C) out of which inferences may be suggested regarding potential association between the genotype and the phenotype by comparing $\theta_0(i)$ to $\theta(i)$. Note, the simulation shown in **(A)** adhering to Fisher seminal model is based on a constant sample size of 1000 involving an arbitrary normally distributed phenotype of mean and variance 68 and 4 units, respectively. Each microstate is normally distributed with a gene effect identical to the standard deviation of the phenotype but without dominance. The frequency of the genotypes aa (red), Aa/aA (Grey) and AA (blue) are 64%, 32% and 4%, respectively and within Hardy-Weinberg ratio.

Figure 2: Linked methionine and propionate metabolism adapted from Clare et al. (2019) where all metabolites studied for this study are in red. The methionine cycle facilitates the re-methylation of homocysteine (Hcy) to methionine (Met) and ultimately S-adenosylmethionine (**SAM**) with methyl (CH_3) groups donated either from folate (5-mTHF) or betaine (trimethylglycine; **TMG**), thus leading to the formation of dimethylglycine (**DMG**). Methylcobalamin (**mB12**) serves as a cofactor for the reduction of the inactive form of methionine synthase to its active state (MTR), which then transfers a methyl group from 5-mTHF to Hcy. The linked metabolism of propionate (**PPA**) to succinate (an intermediary metabolite in the tricarboxylic cycle) requires adenosylcobalamin (**aB12**), which serves as a cofactor for methylmalonyl-CoA-mutase (MUT) leading to the generation of succinyl-CoA and methylmalonic acid (**MMA**) in this pathway. Other intermediary metabolites and enzymes listed: glycine (Gly), sarcosine (Sar), S-adenosylhomocysteine (SAH), tetrahydrofolate (THF), serine (Ser), cystathionine (Cth), cysteine (Cys), alpha-ketobutyrate (α-KB), methylmalonic acid (MMA); Betaine homocysteine methyltransferase (BHMT), Methionine adenosyl-transferase (MAT), Glycine methyl-transferase (GNMT), Adenosyl-homocysteinase (AHCY), Cystathionine beta-synthase (CBS), cystathionine gamma-lyase (Cth).

Figure 3: **(A-left panel)** Simulations of genetic paths corresponding to null hypotheses using GIFT as a method. The data used for the simulation are given in Table-1. **(A-right panel)** Simulations of genetic paths corresponding to null hypotheses when the sample size is divided or multiplied by a factor two. **(B)** Representation of $\Delta\theta_0(i) = \theta_0(i) - \langle\theta_0(i)\rangle$ for the microstates data as given in Table-1. **(C)** Plots of the standard deviation normalised by the square root of the sample size and where the position is also normalised by the sample size.

Figure 4: A sample of genetic paths selected from Dataset-1. The details of the different SNPs displayed are given in Table 2.

Figure 5: Analysis of averages (GWAS) for SNP1-6 (see Fig.4 and Table-2). Values for the size/gene effects (a) and dominances (d) are given in Table 2.

Figure 6: To provide a p-value extracting genotype-phenotype associations in an exhaustive manner for both GWAS and GIFT a method concentrating on the largest and smallest extreme values of the genetic path was focused upon. This method can be applied to paraboloid (GWAS or GIFT-like) **(A)** and sigmoid (GIFT-like) **(B)** genetic paths. The overall idea consists in determining how many paths N_1, N_2 and N_3 can be generated from the respective interval of positions Δi_1, Δi_2 and Δi_3 given that the constraints for the extrema are Φ_1 and Φ_2. Then a p-value (p_{GIFT}) can be determined as seen in the text. **(C)** Using simulations (K=1000 replicates) a statistic of p_{GIFT} for the null hypothesis can be generated using theoretic SNPs (Table-1). Simulations demonstrate that p_{GIFT} is relatively independent of the microstate's frequencies upon which a 99% (upper dashed line) and 95% (lower dashed line) interval confidences can be generated.

Figure 7: Manhattan plots based on p-values obtained by GWAS **(A)** and GIFT **(B)** demonstrating significant differences between the methods concerning potential genotype-phenotype associations. Note that the presence of a chromosome '0' results from the fact that some SNPs identified by (Matika et al., 2016) were not allocated to specific chromosomes/genomic positions due to lack of information at the time. A fathom chromosome (chromosome zero) was created to allocate those SNPs. **(C)** Venn-diagram representing the most significant SNPs (99%-confidence interval) by GWAS and GIFT. One SNP (OAR6_40311379) demonstrated a large p-value for GWAS and a small p-value for GIFT. A representation of its genetic path **(D-left)** did not underscore any 'parabolic' or 'sigmoidal' associations. As it turned out this SNP was a false-positive by GWAS since the difference between the phenotypic means was not significative **(D-right)**. **(E)** The 100 most significant SNPs by GWAS and GIFT were extracted, and their p-values plotted against each other. The dashed lines represent the threshold applied for GWAS (blue dashed line) and GIFT (red dashed line). The SNP OAR6_40311379 pointed by the black arrow is the single one standing out in Q_1 confirming its false-positive status. **(F)** The biotypes of the most significant SNPs by GIFT and GWAS are shown.

Figure 8: (A) Comparison of the information extracted by GWAS and GIFT using Manhattan plots for the metabolites presented in red in Fig.2. We recall the acronyms, S-adenosyl methionine (SAM), methylcobalamin (mB12), adenosylcobalamin (aB12), trimethylglycine (TMG), dimethylglycine (DMG), propionate (PPA) and methylmalonic acid (MMA). It should be noted that due to inherent difficulty linked to the measure of metabolite the sample sizes were not similar across metabolites, that is the values for N differ between the Manhattan plots (SAM: N=344; mB12: N=183; aB12: N=338; DMG: N=338; TMG: N=340; MMA: N=348; PPA: N=345). **(B)** Biotypes corresponding to the most significant SNPs for each metabolite as determined by GIFT (a detailed list of information concerning those SNPs in given in supplementary material 4).

Figure 1

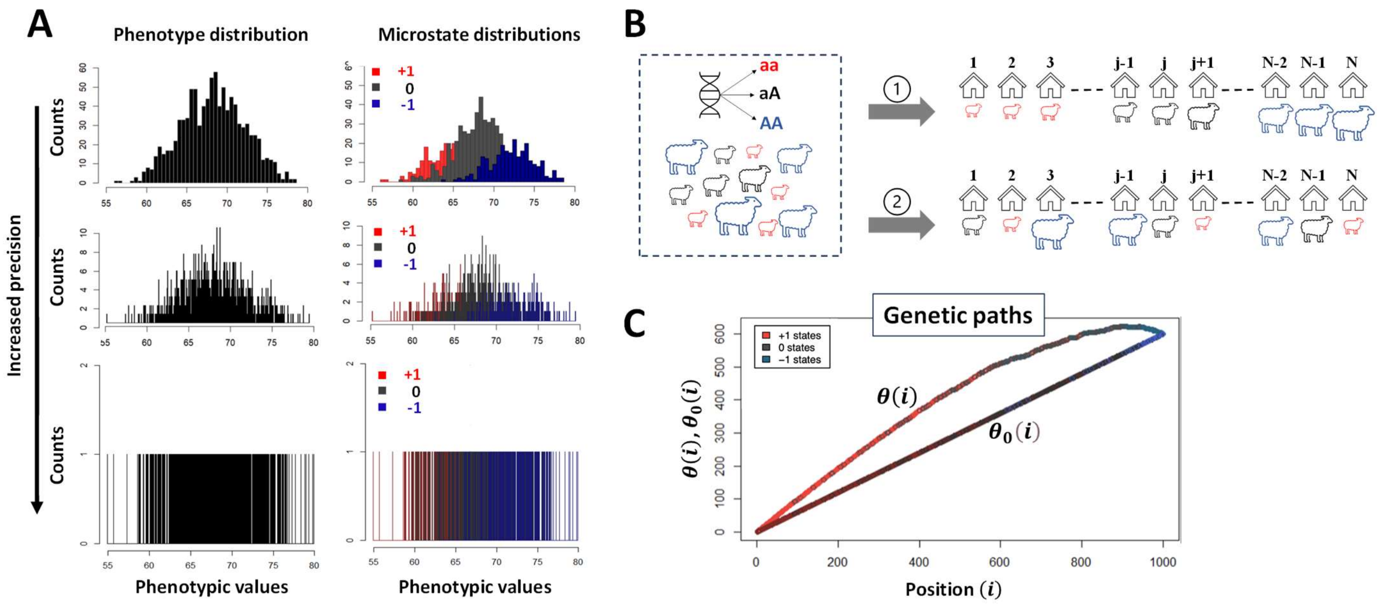
A
Phenotype distribution
Microstate distributions
Increased precision
Counts
Counts
Counts
+1
0
-1
+1
0
-1
+1
0
-1
Phenotypic values
Phenotypic values
B
aa
aA
AA
1
2
1 2 3 j-1 j j+1 N-2 N-1 N
1 2 3 j-1 j j+1 N-2 N-1 N
C
Genetic paths
+1 states
0 states
−1 states
$\theta(i)$
$\theta_0(i)$
$\theta(i), \theta_0(i)$
Position (i)

Figure 2

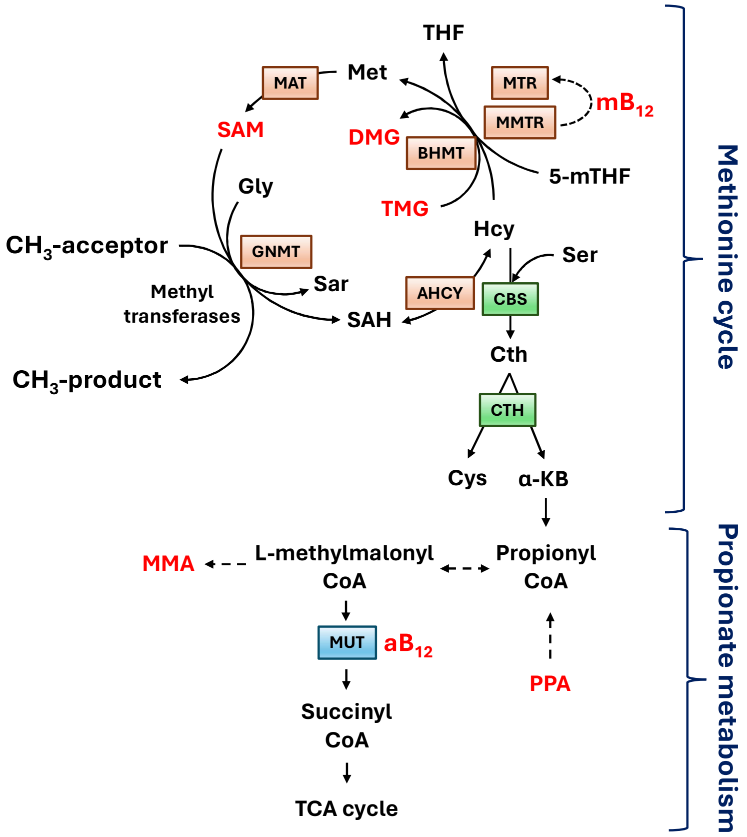
THF
Met
MAT
MTR
MMTR
mB$_{12}$
SAM
DMG
BHMT
5-mTHF
Gly
TMG
Hcy
CH$_3$-acceptor
GNMT
Ser
Sar
AHCY
CBS
Methyl transferases
SAH
Cth
CH$_3$-product
CTH
Cys
α-KB
Methionine cycle
MMA
L-methylmalonyl CoA
Propionyl CoA
MUT
aB$_{12}$
PPA
Succinyl CoA
TCA cycle
Propionate metabolism

Figure 3

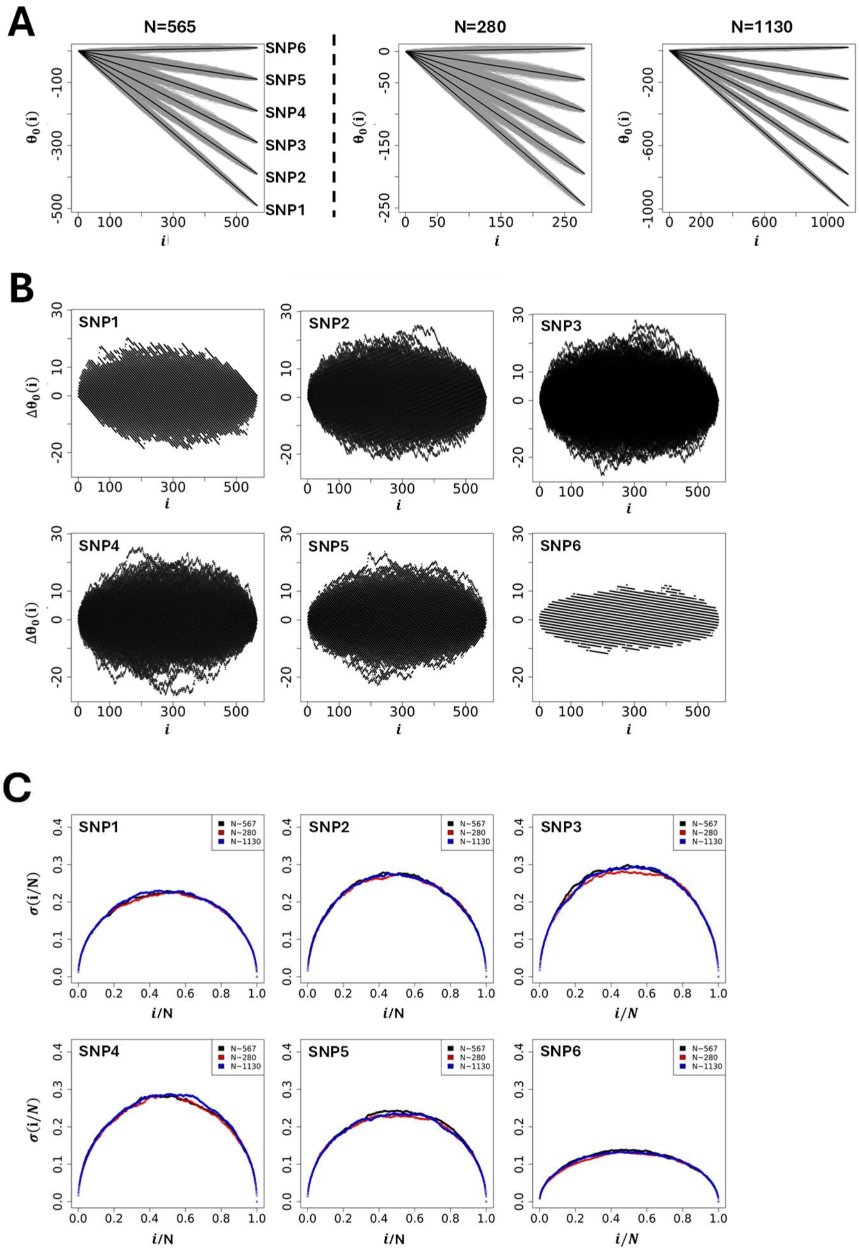
A
N=565
N=280
N=1130
SNP6
SNP5
SNP4
SNP3
SNP2
SNP1
$\theta_0(i)$
i
B
SNP1
SNP2
SNP3
SNP4
SNP5
SNP6
$\Delta\theta_0(i)$
i
C
SNP1
SNP2
SNP3
SNP4
SNP5
SNP6
N~567
N~280
N~1130
$\sigma(i/N)$
i/N

Figure 4

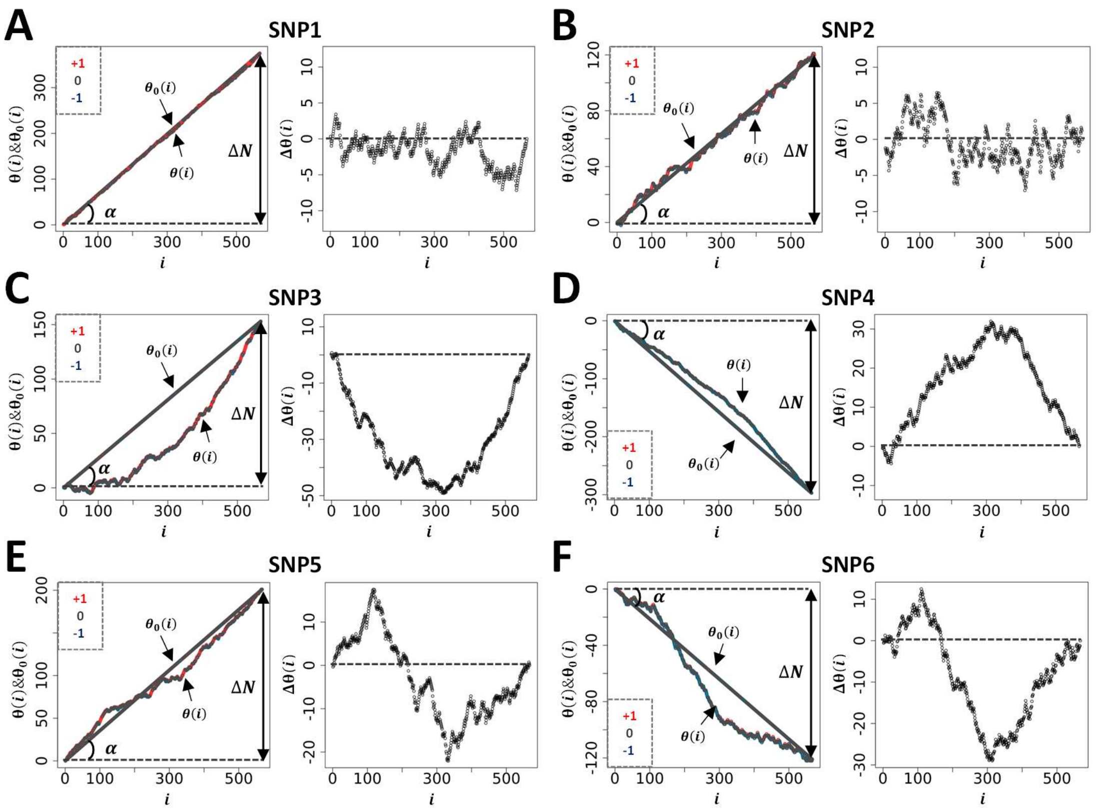
A
SNP1
B
SNP2
C
SNP3
D
SNP4
E
SNP5
F
SNP6
+1
0
-1
$\theta_0(i)$
$\theta(i)$
α
ΔN
$\theta(i)\&\theta_0(i)$
$\Delta\theta(i)$
i
0
100
300
500

Figure 5

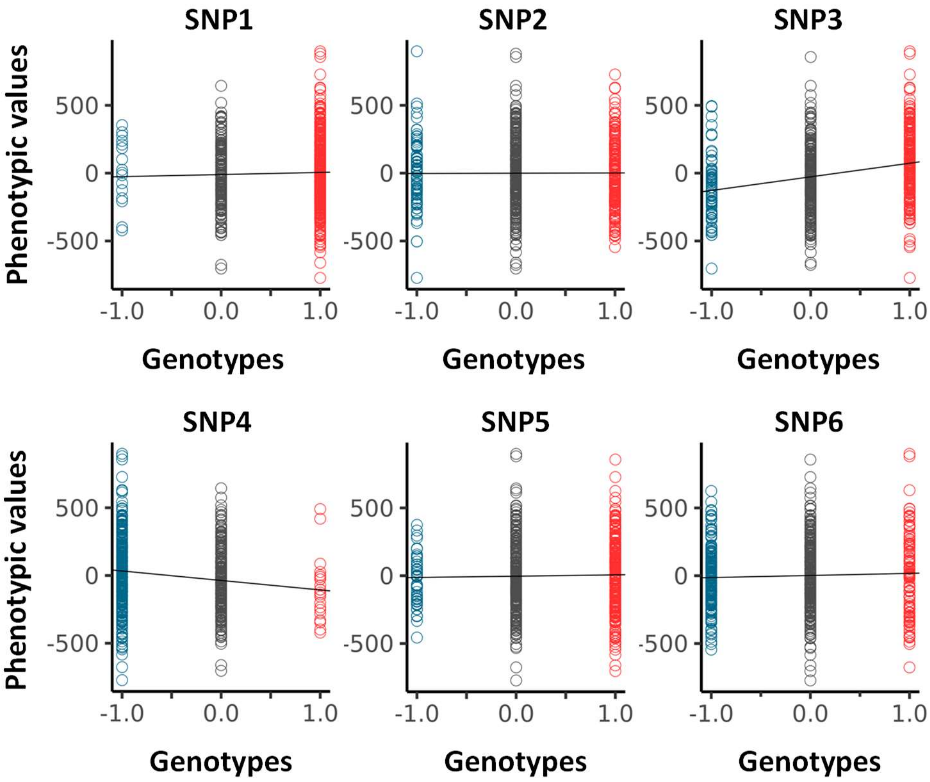
SNP1
SNP2
SNP3
SNP4
SNP5
SNP6
Phenotypic values
Phenotypic values
500
0
-500
-1.0
0.0
1.0
Genotypes

Figure 6

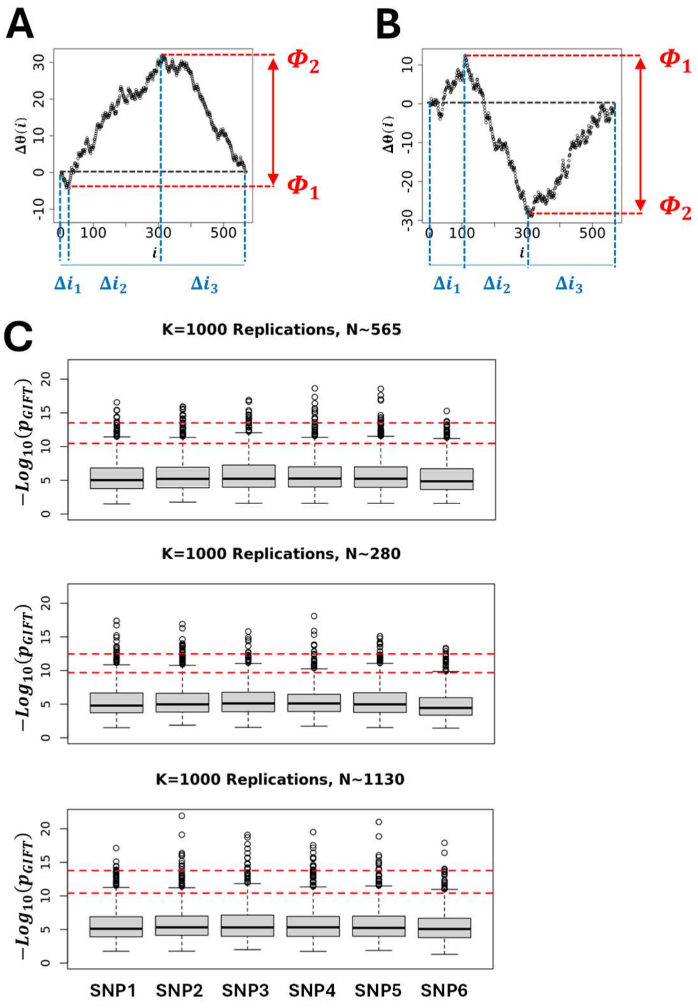

K=1000 Replications, N~565

K=1000 Replications, N~280

K=1000 Replications, N~1130

Figure 7

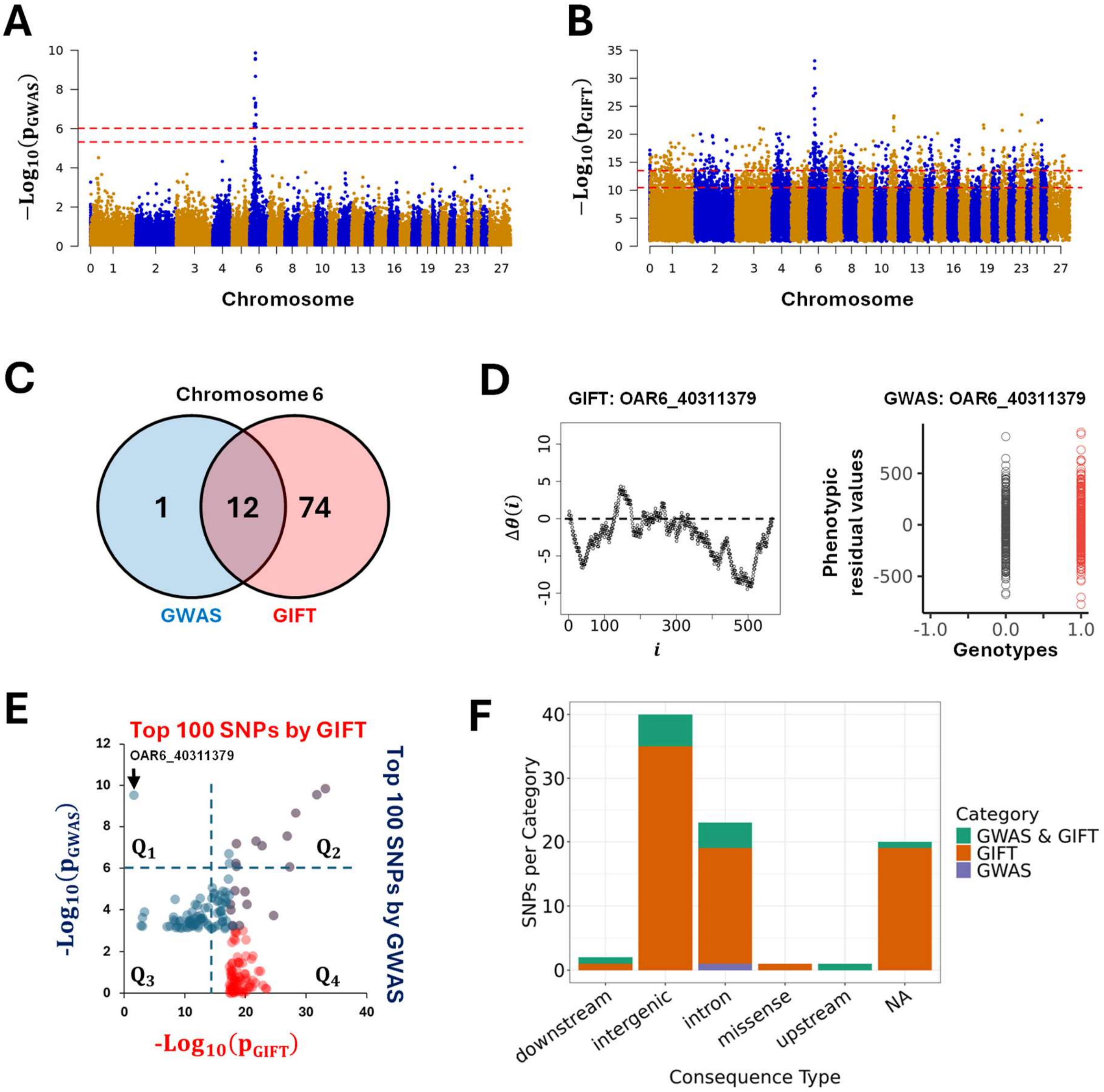
A
$-\mathrm{Log}_{10}(\mathrm{p}_{\mathrm{GWAS}})$
0
2
4
6
8
10
0 1 2 3 4 6 8 10 13 16 19 23 27
Chromosome
B
$-\mathrm{Log}_{10}(\mathrm{p}_{\mathrm{GIFT}})$
0
5
10
15
20
25
30
35
0 1 2 3 4 6 8 10 13 16 19 23 27
Chromosome
C
Chromosome 6
1
12
74
GWAS
GIFT
D
GIFT: OAR6_40311379
$\Delta\theta(i)$
-10
-5
0
5
10
0 100 300 500
i
GWAS: OAR6_40311379
Phenotypic residual values
-500
0
500
-1.0 0.0 1.0
Genotypes
E
Top 100 SNPs by GIFT
OAR6_40311379
$-\mathrm{Log}_{10}(\mathrm{p}_{\mathrm{GWAS}})$
0
2
4
6
8
10
12
Q_1
Q_2
Q_3
Q_4
0 10 20 30 40
$-\mathrm{Log}_{10}(\mathrm{p}_{\mathrm{GIFT}})$
Top 100 SNPs by GWAS
F
SNPs per Category
0
10
20
30
40
downstream
intergenic
intron
missense
upstream
NA
Consequence Type
Category
GWAS & GIFT
GIFT
GWAS

Figure 8

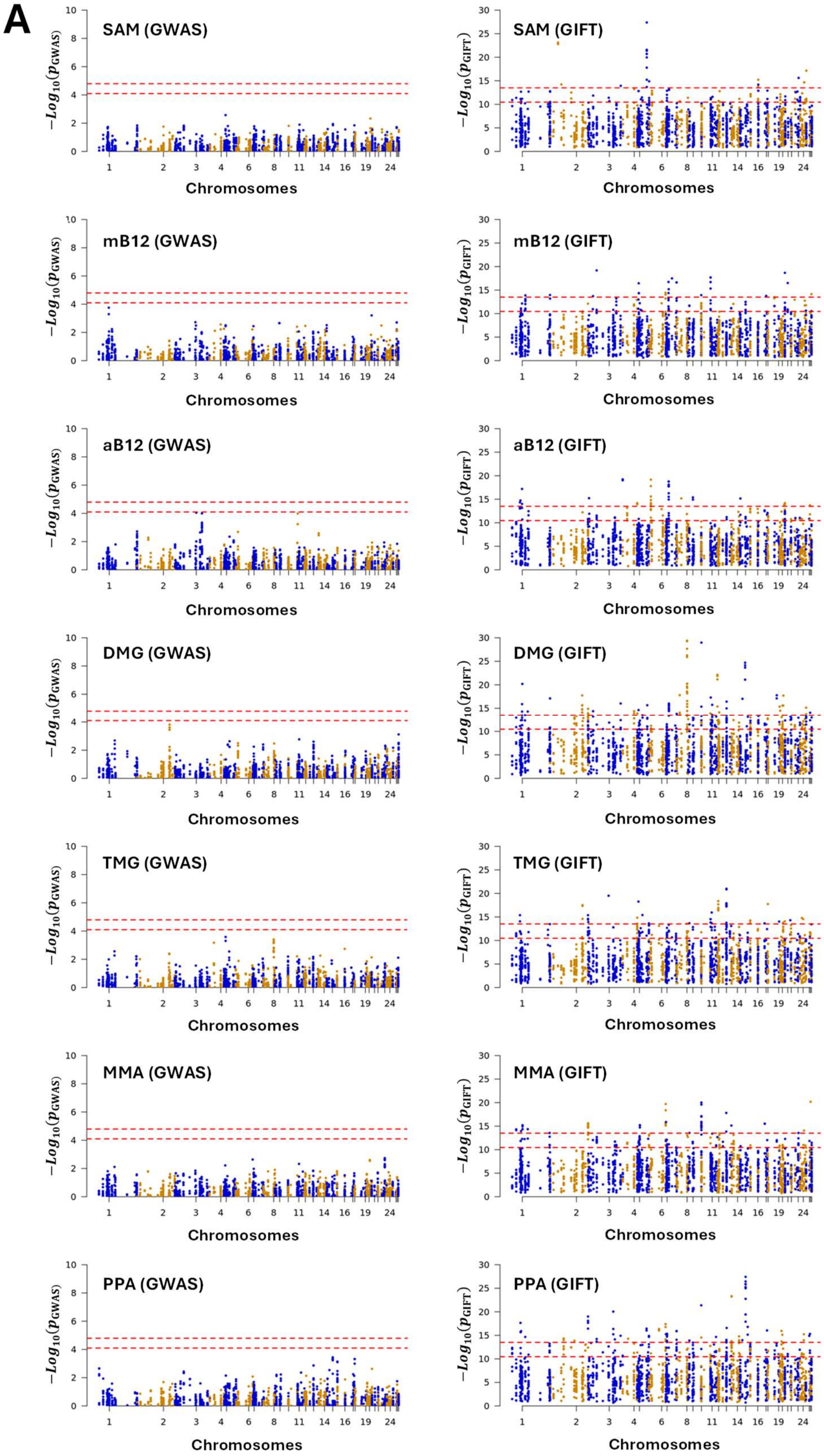
A
SAM (GWAS)
SAM (GIFT)
mB12 (GWAS)
mB12 (GIFT)
aB12 (GWAS)
aB12 (GIFT)
DMG (GWAS)
DMG (GIFT)
TMG (GWAS)
TMG (GIFT)
MMA (GWAS)
MMA (GIFT)
PPA (GWAS)
PPA (GIFT)
$-Log_{10}(p_{GWAS})$
$-Log_{10}(p_{GIFT})$
0
2
4
6
8
10
0
5
10
15
20
25
30
1
2
3
4
6
8
11
14
16
19
24
Chromosomes

Figure 8 continued

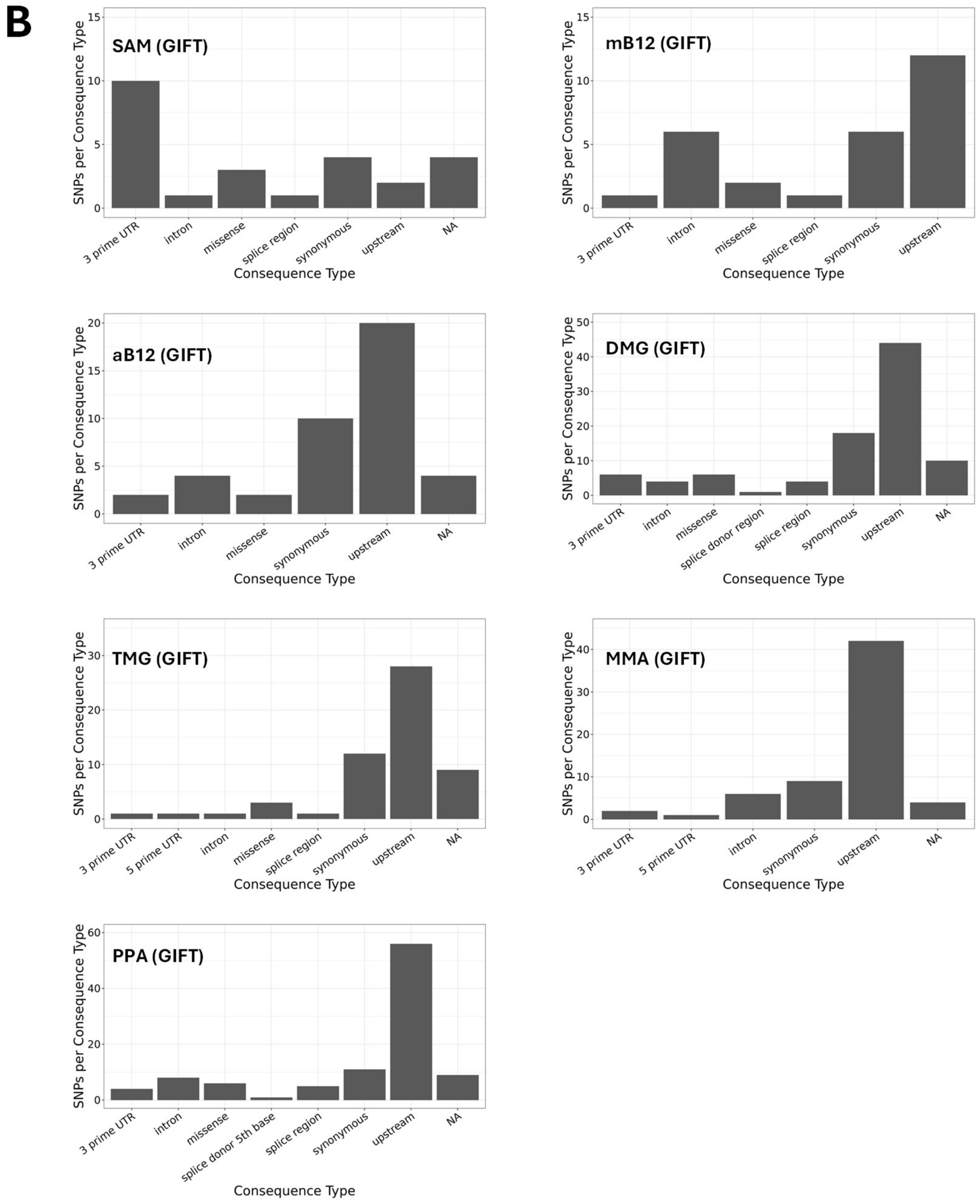
B
SAM (GIFT)
SNPs per Consequence Type
3 prime UTR
intron
missense
splice region
synonymous
upstream
NA
Consequence Type
mB12 (GIFT)
SNPs per Consequence Type
3 prime UTR
intron
missense
splice region
synonymous
upstream
Consequence Type
aB12 (GIFT)
SNPs per Consequence Type
3 prime UTR
intron
missense
synonymous
upstream
NA
Consequence Type
DMG (GIFT)
SNPs per Consequence Type
3 prime UTR
intron
missense
splice donor region
splice region
synonymous
upstream
NA
Consequence Type
TMG (GIFT)
SNPs per Consequence Type
3 prime UTR
5 prime UTR
intron
missense
splice region
synonymous
upstream
NA
Consequence Type
MMA (GIFT)
SNPs per Consequence Type
3 prime UTR
5 prime UTR
intron
synonymous
upstream
NA
Consequence Type
PPA (GIFT)
SNPs per Consequence Type
3 prime UTR
intron
missense
splice donor 5th base
splice region
synonymous
upstream
NA
Consequence Type